

Luminance-GS: Adapting 3D Gaussian Splatting to Challenging Lighting Conditions with View-Adaptive Curve Adjustment

Ziteng Cui¹, Xuangeng Chu¹, Tatsuya Harada^{1,2}

¹ The University of Tokyo ² RIKEN AIP

(cui, xuangeng.chu, harada)@mi.t.u-tokyo.ac.jp

Abstract

Capturing high-quality photographs under diverse real-world lighting conditions is challenging, as both natural lighting (e.g., low-light) and camera exposure settings (e.g., exposure time) significantly impact image quality. This challenge becomes more pronounced in multi-view scenarios, where variations in lighting and image signal processor (ISP) settings across viewpoints introduce photometric inconsistencies. Such lighting degradations and view-dependent variations pose substantial challenges to novel view synthesis (NVS) frameworks based on Neural Radiance Fields (NeRF) and 3D Gaussian Splatting (3DGS).

To address this, we introduce **Luminance-GS**, a novel approach to achieving high-quality novel view synthesis results under diverse challenging lighting conditions using 3DGS. By adopting per-view color matrix mapping and view adaptive curve adjustments, Luminance-GS achieves state-of-the-art (SOTA) results across various lighting conditions—including low-light, overexposure, and varying exposure—while not altering the original 3DGS explicit representation. Compared to previous NeRF- and 3DGS-based baselines, Luminance-GS provides real-time rendering speed with improved reconstruction quality. The source code is available at ¹.

1. Introduction

In recent years, Neural Radiance Field (NeRF) and Gaussian Splatting (3DGS) based methods [3, 4, 10, 18, 29, 34, 35, 38, 41, 44, 62] have made significant strides in reconstructing realistic 3D scenes and generating coherent novel views. The impressive performance of NeRF and 3DGS has found applications across various fields, including augmented and virtual reality (AR/VR), computational photography, medical imaging, and autonomous driving, etc. Both NeRF- and 3DGS-based methods aim to synthesize novel views by learning from existing multi-view images, capturing

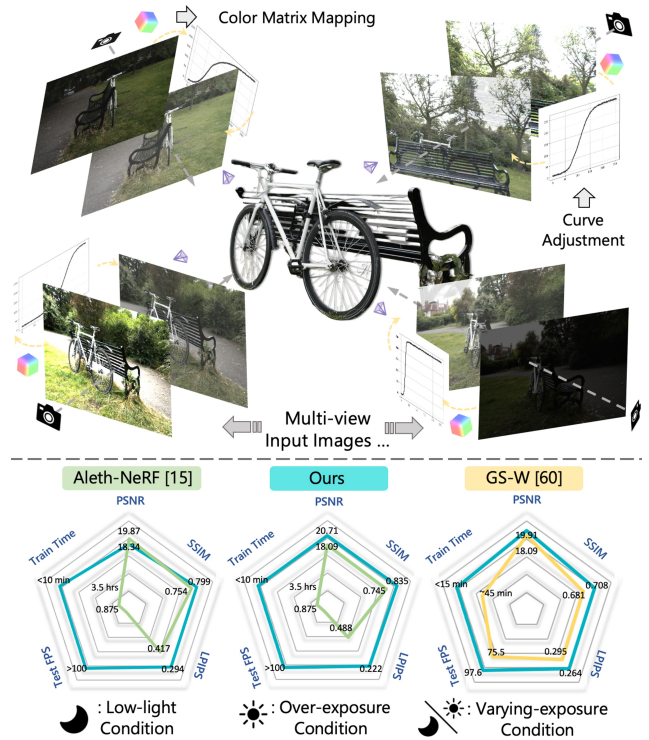


Figure 1. *Up*: The core idea of Luminance-GS is to perform view-adaptive adjustments for images from each viewpoint, including color matrix mapping and curve adjustment. *Down*: Compare with previous SOTA solutions [15, 60], our approach achieves superior performance and efficiency across different lighting conditions.

ing consistent geometric information and simulating non-Lambertian effects. Despite their success under normal, uniform lighting, these methods often struggle with real-world challenging lighting conditions (e.g., low-light, varying camera exposure), which is primarily due to the lightness distortion caused by the environment or camera sensor limitations [42, 52], and the inherent lack of illumination modeling in both NeRF and 3DGS methods [37, 47]. To make matters worse, *de facto* results [15, 24, 67] also show that using 2D image restoration methods [1, 14, 23, 39] to

¹<https://github.com/cuiziteng/Luminance-GS>

pre-process multi-view training images is also ineffective, as 2D models often fail to preserve 3D consistency, leading to floaters and artifacts during rendering.

To ensure high-quality view synthesis under challenging lighting conditions, NeRF-W [40] and its following works [11, 32, 56, 60] typically learn a separate appearance embedding for each viewpoint, effectively isolating the lighting information specific to each camera view. However, they are limited to capturing only the lighting conditions present in input images, restricting the models’ ability to adapt to a new lighting condition during rendering (e.g., achieving low-light enhancement). For low-light conditions, NeRF-based solutions [15, 24, 52, 67] tend to incorporate different assumptions in volume rendering stage, enabling unsupervised lightness restoration while maintaining 3D multi-view consistency. For instance, LL-NeRF [24] decomposes NeRF’s color MLP to separate each volume particle into view-dependent and view-independent components for distinct processing, meanwhile Aleth-NeRF [15] introduces an additional MLP branch to learn “concealing fields”, simulating low-light conditions as occlusions, which are later removed during testing to enhance output.

However, these solutions do not generalize well to explicit representations such as 3DGS [29], which employs rasterization to store the color of geometric primitives in an explicit radiance field, removing the need of implicit representation and MLP structure, thus offers substantial advantages over NeRF-based methods in both inference speed and training time [7, 10, 20, 29]. This raises a key question: How can we leverage the efficiency of 3DGS’s explicit rendering while also ensuring robust reconstruction quality under diverse and challenging lighting conditions?

Our solution, **Luminance-GS**, avoids altering the original 3DGS explicit representation or imposing additional lighting assumptions. Instead, we employ a simple yet effective image processing technique: curve adjustment. We use different tone curves to map input images under varying lighting conditions (e.g., low-light, overexposure) to a consistently well-lit output, ensuring view consistency and supporting 3DGS training. To achieve this, we design two sub-solutions: per-view color matrix mapping and view-adaptive curve adjustment. For each viewpoint, we project the image into a suitable representation using a specific matrix, followed by curve adjustment tailored to the current view’s lighting condition (see Fig. 1 *Up*). During training time, the projection matrix and view-adaptive curve would be jointly optimized with other 3DGS parameters. Finally, several unsupervised loss functions are introduced to maintain the shape of the curve while ensuring view alignment across images from different viewpoints. Extensive experiments under various lighting conditions demonstrate our algorithm’s state-of-the-art (SOTA) performance, achieving significant advantages over previous methods in both effi-

ciency and quality (see Fig. 1 *Down*). The contributions of our work can be summarized as follows:

- We introduce Luminance-GS, a novel framework that extends 3DGS to handle novel view synthesis under diverse challenging lighting conditions. By using per-view color matrix mapping and view-adaptive curve adjustment, we achieve view-aligned, normal-light outputs from images captured under varying lighting conditions.
- We introduce unsupervised loss functions to guide both curve mapping and 3DGS training. Additionally, curve mapping is applied only during training to generate pseudo-enhanced images, saving a significant amount of testing time.
- Our method achieves state-of-the-art (SOTA) results in various lighting conditions (low-light, overexposure, and varying exposure), substantially improving both speed and rendering quality compared to previous methods.

2. Related Works

2.1. 3D Gaussian Splatting

Neural Radiance Fields (NeRF) [41] have greatly advanced the field of novel view synthesis (NVS), but NeRF-based methods [3, 4, 13, 18, 34, 35, 41, 66] still struggle with real-time rendering, as they require multiple queries to render a single pixel, which limits their practical use. Recently, 3D Gaussian Splatting (3DGS) [29] has emerged as a more efficient alternative, enabling real-time NVS with performance comparable to top NeRF methods like Mip-NeRF 360[3]. The efficiency of 3DGS comes from its explicit scene representation, using learnable anisotropic 3D Gaussians and differentiable splatting with tile-based rasterization.

Building on this, several works have been introduced to improve the rendering quality, robustness, and generalization of 3DGS, as well as to explore its applications in specific areas [6, 10, 12, 21, 22, 25, 30, 37, 38, 50]. For example, 2DGS [25] simplifies the 3D volume into 2D oriented planar Gaussian disks to capture more accurate surface normals. MVSplat [12] and MVSGaussian [38] focus on achieving generalizable, feed-forward NVS. Additionally, X-Gaussian [6] applies 3DGS to X-ray NVS, demonstrating its effectiveness in sparse-view CT reconstruction.

2.2. Curve Adjustment in Image Processing

Curve-based adjustment modifies an image’s tonal range or brightness by altering pixel values with a tone curve, which is commonly applied in commercial image software like Adobe Lightroom[®]. In earlier time, predefined curves (e.g., power curves, S-curves) were often used, with experts manually adjusting them to enhance detail and align with human visual perception [5, 28, 46, 59].

In the deep learning era, data-driven solutions have become popular, using curves learned from datasets to per-

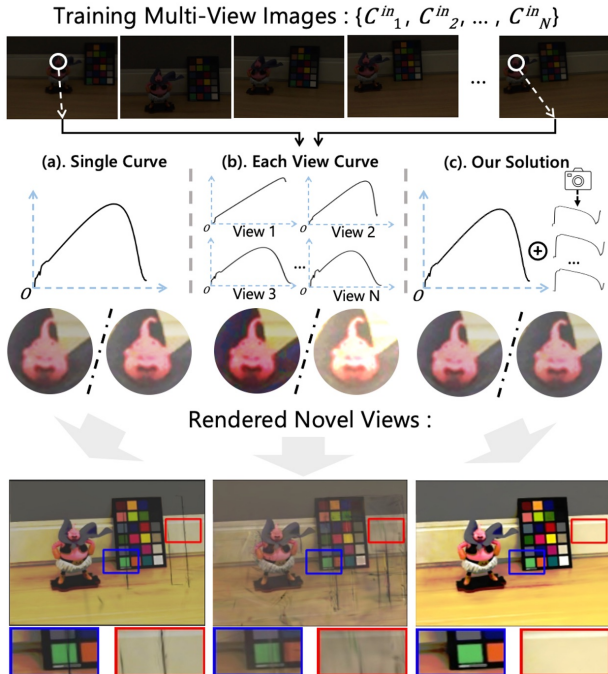


Figure 2. Ablation analysis of different curve settings in LOM dataset [15] “*buu*” scene: (a). All views low-light images share a single curve, (b). each view low-light image adopts an individual trainable curve and (c). our Luminance-GS solutions.

form global or local adjustments on images [9, 16, 23, 26, 31, 33, 43, 48, 51, 55]. For example, CURL [43] learns curves across multiple color spaces (RGB, HSV, CIE Lab) for targeted adjustments, and Zero-DCE [23] estimates pixel-wise, high-order curves, leveraging unsupervised loss functions for low-light enhancement. Recently, NamedCurves [48] decomposes images based on the color naming system and applies Bézier curves for each color category. Unlike these 2D methods, our approach applies view-dependent curve adjustments across multiple views. We aim to correct brightness and contrast while ensuring 3D consistency, facilitating stable 3DGS training.

2.3. NVS in Challenging Lighting Conditions

While NeRF and 3DGS-based methods have achieved significant success in novel view synthesis (NVS) under normal lighting, a parallel line of research has emerged to enhance NVS performance under diverse, challenging real-world lighting conditions. Methods like NeRF-W [40] and follow-up works [11, 17, 32, 56, 60] address NeRF rendering under inconsistent lighting and the presence of occluding objects. For low-light conditions, RAW-NeRF [42] and its extensions [27, 36, 49, 63] improve details by training with high dynamic range (HDR) camera RAW data. However, these methods are constrained by challenges in RAW data capture and storage, as well as longer training times.

Similar to our work, several studies focus on address-

ing NVS in challenging lighting conditions using sRGB inputs [15, 24, 45, 52, 53, 57, 67], like Aleth-NeRF [15] introduces the concept of “concealing field” to control lightness, Bilarf [52] optimizes 3D bilateral grids to simulate camera pipeline effects for each view, and Thermal-NeRF [53] fuses low-light sRGB images with thermal images to achieve normal-light reconstruction results. Unlike previous methods, our Luminance-GS focuses more on using curve adjustment to generate and optimize pseudo-enhanced images. Moreover, our method can adapt to varying different challenging lighting conditions without modifying any training strategies or hyper-parameters.

3. Proposed Method

3.1. Preliminary: 3D Gaussian Splatting

3D Gaussian Splatting (3DGS) [29] is an explicit point-based 3D representation with a set of Gaussians $\{G_1, \dots, G_M\}$. Each Gaussian G_i is characterized by center position μ_i , covariance matrix Σ_i , spherical harmonics coefficients c_i (which represent color) and opacity o_i . During rendering, each Gaussian will be projected and accumulated on the 2D image plane with camera parameters [68]:

$$\hat{C}(x) = \sum_{i=1}^N c_i o'_i \prod_{j=1}^{i-1} (1 - o'_j), \quad (1)$$

where N is the set of Gaussians (sorted along the depth after projection) that affect the pixel x , The o'_i is the opacity after multiplying with projected Σ_i . Then 3D Gaussians will be optimized through a mixed loss function \mathcal{L}_{3DGS} between the predicted image \hat{C} and ground truth C :

$$\mathcal{L}_{3DGS}(\hat{C}, C) = \lambda \mathcal{L}_{DSSIM}(\hat{C}, C) + (1 - \lambda) \mathcal{L}_1(\hat{C}, C), \quad (2)$$

where \mathcal{L}_{DSSIM} denotes DSSIM loss and \mathcal{L}_1 denotes L1 loss, λ is a balancing weight. We refer more details such as adaptive Gaussian densification to original 3DGS paper [29].

3.2. Luminance-GS Pipeline

Fig. 3 provides an overview of **Luminance-GS**. Beginning with SfM points, we model a set of 3D Gaussians, $\{G_1, \dots, G_M\}$, with color attributes c_i to render multi-view images $\{C_1^{in}, C_2^{in}, \dots, C_N^{in}\}$, captured under challenging lighting conditions (e.g., low-light, varying exposure).

Within original 3DGS framework, we additionally learn a set of color adjustment parameters \mathbf{a}_i and \mathbf{b}_i , jointly optimized with other 3DGS parameters. \mathbf{a}_i and \mathbf{b}_i transform color c_i into c_i^{out} using a least-squares formula [32]:

$$c_i^{out} = \mathbf{a}_i \cdot c_i + \mathbf{b}_i, \quad (3)$$

3D Gaussians $G_{i \in (1, M)}$ are simultaneously applied alongside the transformed colors c_i^{out} to render pseudo-enhanced

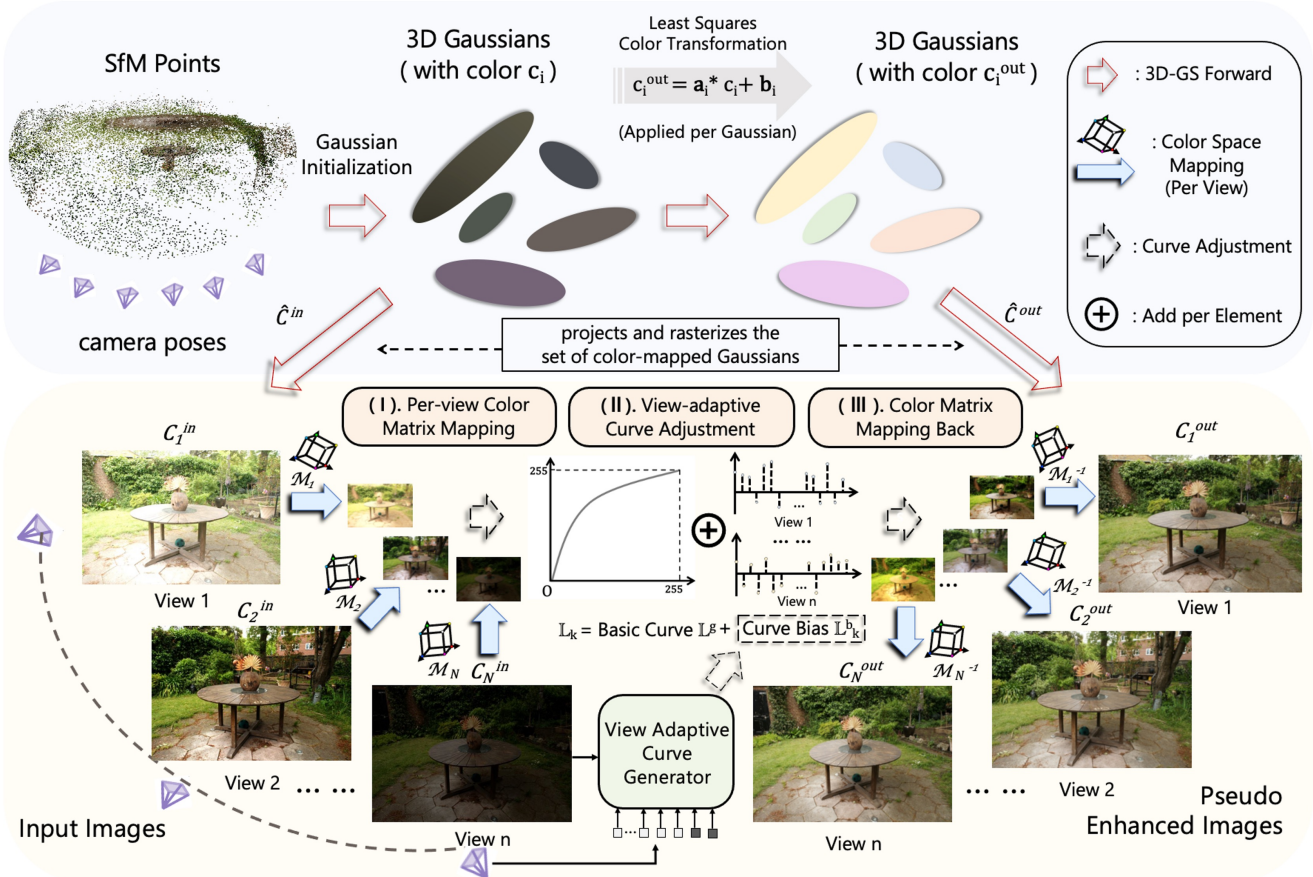


Figure 3. **Overview of Luminance-GS pipeline.** *Up*: Our method jointly optimize 3D Gaussians with two set of color attributes c_i and c_i^{out} to render out input images C_i^{in} and pseudo enhanced images C_i^{out} . *Down*: To translate C_i^{in} in to view-aligned enhanced C_i^{out} , we design 3 steps: (I). per-view color matrix mapping, (II). view-adaptive curve adjustment and (III). color matrix mapping back.

images C_i^{out} , which are translated from the input images C_i^{in} . During training time, Luminance-GS jointly predicts both C_i^{in} and C_i^{out} , leading to an extension of Eq. 1 as:

$$\begin{aligned} \hat{C}^{in}(x) &= \sum_{i=1}^N c_i o_i' \prod_{j=1}^{i-1} (1 - o_j') \\ \hat{C}^{out}(x) &= \sum_{i=1}^N c_i^{out} o_i' \prod_{j=1}^{i-1} (1 - o_j'). \end{aligned} \quad (4)$$

During inference time, 3D Gaussians would only applied alongside c_i^{out} to render out novel view $\hat{C}^{out}(x)$. In following section, we would explain how to convert the input images $\{C_1^{in}, C_2^{in}, \dots, C_N^{in}\}$ into view-aligned, pseudo-enhanced images $\{C_1^{out}, C_2^{out}, \dots, C_N^{out}\}$.

3.2.1. Problem Setup

Given multi-view images $C_{k \in (1, N)}^{in}$ captured under challenging lighting conditions (e.g., low-light, overexposure, or varying exposure), our primary goals for effective 3DGS training—which requires uniform lighting for optimal performance—are: (1) restoring lighting to approximate nor-

mal conditions, and (2) ensuring consistent illumination across views to preserve multi-view consistency in 3D. We adopt a straightforward curve adjustment process to achieve these two goals, the basic operation maps input pixel values to corresponding output values, enabling brightness and contrast adjustments [5, 48, 59]. By applying tone curves to map the input images $C_{k \in (1, N)}^{in}$ to a set of uniformly normal-light images $C_{k \in (1, N)}^{out}$, we aim to ensure color and luminance consistency across views $k \in (1, N)$, thereby facilitating 3DGS novel view synthesis.

In our implementation, we initially applied a single tone curve to all input views $C_{k \in (1, N)}^{in}$, however, as illustrated in Fig. 2(a), even under relatively consistent low-light condition, single curve approach introduced view inconsistencies and rendering artifacts. We then experimented with assigning a unique curve to each view, but this only worsened the problem (see Fig. 2(b)), the individual curves quickly became unstable and overfitted during training, resulting in pronounced inter-view discrepancies and significantly degraded rendering quality. To address this, we developed two solutions: Per-view Color Mapping

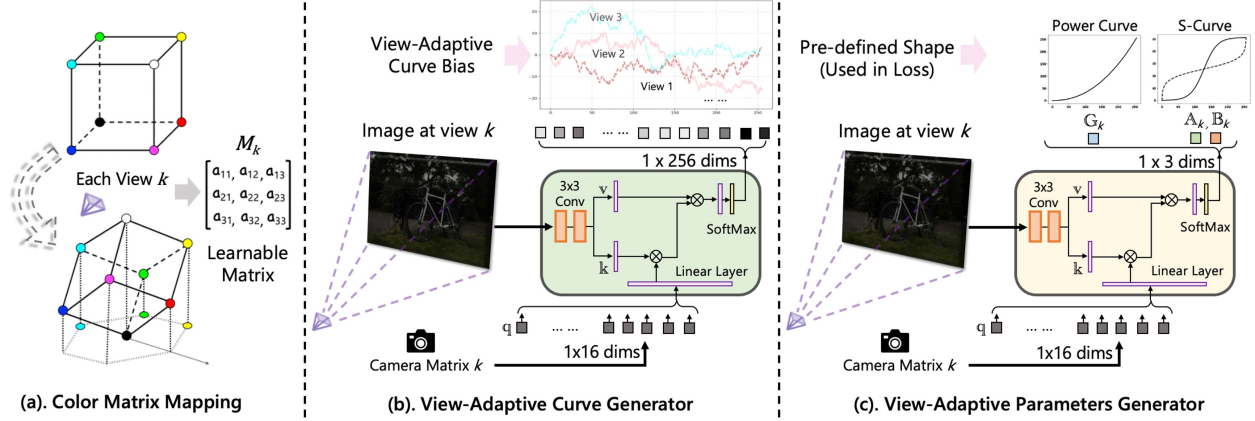


Figure 4. (a). Per-view Color Matrix Mapping with learnable matrix \mathcal{M}_k . (b). Structure of view-adaptive curve generator, given input image C_k^{in} and corresponding camera pose to predict curve bias \mathbb{L}_k^b . (c). Structure of view-adaptive parameters generator.

and View-adaptive Curve Adjustment. With additional loss constraints, our Luminance-GS model effectively resolves these issues, achieving high-quality rendering results (see Fig. 2(c)). The detailed explanations are as follows.

3.2.2. Per-view Color Matrix Mapping

In multi-view scenes, differences in lighting and camera exposure settings often result in color variations among images [32, 60]. To address this, we first learn a unique matrix \mathcal{M}_k for each view k . Before curve adjustment, each input image is projected into its suitable view-dependent coordinate system via \mathcal{M}_k [16]. A demonstration of color matrix mapping can be found in Fig. 4(a).

As indicated by the blue arrow in Fig. 3, given input image $C_{k \in (1, N)}^{in}(r, g, b)$ in the RGB color space $\mathbb{I}(R, G, B)$, for each view k , we optimize a per-view 3×3 invertible matrix \mathcal{M}_k . Initially set as an identity matrix, \mathcal{M}_k is jointly optimized with other 3DGS parameters. We define the color matrix mapping process as F , shown as follow equation:

$$\begin{aligned}
 F(C_k^{in}) &= C_k^{in} \cdot \mathcal{M}_k \\
 &= [C_k^{in}(r), C_k^{in}(g), C_k^{in}(b)] \cdot \begin{bmatrix} a_{11} & a_{12} & a_{13} \\ a_{21} & a_{22} & a_{23} \\ a_{31} & a_{32} & a_{33} \end{bmatrix} \\
 &= [C_k^{in}(r'), C_k^{in}(g'), C_k^{in}(b')],
 \end{aligned} \tag{5}$$

$F(C_k^{in})$ is the output in view k , where RGB channels of input image $C_k^{in}(r), C_k^{in}(g), C_k^{in}(b)$ are transformed by matrix \mathcal{M}_k . Each element $\mathcal{M}_k(a_{ij})$ is a learnable parameter that enables color matrix mapping to adjust view characteristics. The transformed values $C_k^{in}(r'), C_k^{in}(g'), C_k^{in}(b')$, represent the image in the projected coordinate system, ready for subsequent view-adaptive curve adjustments.

3.2.3. View-adaptive Curve Adjustment

For curve design, we first learn a global curve \mathbb{L}^g that is shared across all views $k \in (1, N)$. Then, for each view

k , we learn a curve bias \mathbb{L}_k^b , which is added to the global curve to obtain the final tone curve $\mathbb{L}_k: \mathbb{L}_k = \mathbb{L}^g + \mathbb{L}_k^b$. Here the global curve \mathbb{L}^g helps keep brightness and color tone consistent across all views, which works well in evenly lit environments (see Table.4). Additionally, the view-specific curve bias \mathbb{L}_k^b allows each view to fine-tune its brightness, providing flexibility for individual adjustments.

In our implementation, global curve \mathbb{L}^g is set as a one-dimensional parameter with a length of 256 (ranging from 0 to 255). For curve bias \mathbb{L}_k^b , to avoid overfitting, we incorporate an attention block as a view-adaptive curve generator, inspired by [8, 14]. The detailed structure is shown in Fig. 4(b). For each view k , image C_k^{in} is encoded by two down-scaling convolution layers and two linear layers to produce attention's key and value. Then camera matrix at view k would set as query to calculate cross attention [19] with key and value, followed by a feed-forward network (FFN) that projects the output to a 1×256 dimension \mathbb{L}_k^b .

Afterward, \mathbb{L}_k^b is added to \mathbb{L}^g to produce \mathbb{L}_k , which is then applied to map the image $F(C_k^{in})$ to the output value $\mathbb{L}_k(F(C_k^{in}))$. Finally, the result is multiplied by the inverse of \mathcal{M}_k and mapped back to the RGB color space, generating the pseudo-enhanced image C_k^{out} , as follow:

$$C_k^{out} = \mathbb{L}_k(C_k^{in} \cdot \mathcal{M}_k) \cdot \mathcal{M}_k^{-1}. \tag{6}$$

In next section, we would introduce how to set effective loss functions to control curve \mathbb{L}_k and our model training.

3.3. Optimization Solution

3.3.1. Image-level Loss Constraints

We begin by introducing the image-level loss functions, as shown in Eq.4, Luminance-GS jointly predicts the input multi-view images $C_{k \in (1, N)}^{in}$ and the pseudo-enhanced images $C_{k \in (1, N)}^{out}$ consequently, the regression loss \mathcal{L}_{reg} for Luminance-GS is updated from Eq.2 as follows:

$$\mathcal{L}_{reg} = \mathcal{L}_{3DGS}(\hat{C}^{in}, C^{in}) + \mathcal{L}_{3DGS}(\hat{C}^{out}, C^{out}). \tag{7}$$

Secondly, inspired by Zero-DCE [23], we introduce loss function \mathcal{L}_{spa} , to preserve structural similarity between the predicted enhanced image \hat{C}^{out} and the input image C^{in} . \mathcal{L}_{spa} will compute the difference between the neighboring pixel distances of \hat{C}^{out} and C^{in} , equation as follow:

$$\mathcal{L}_{\text{spa}} = \frac{1}{K} \sum_{x=1}^K \sum_{y \in \Omega(x)} (|\hat{C}^{\text{out}}(x) - \hat{C}^{\text{out}}(y)| - \frac{0.5}{C^{\text{in}}(x)} |(C^{\text{in}}(x) - C^{\text{in}}(y))|)^2. \quad (8)$$

Here, x denotes the pixel location, and $y \in \Omega(x)$ represents neighboring pixels of x . Unlike [15, 23], which set difference parameter to be fixed, we treat it as an adaptive parameter $\frac{0.5}{C^{\text{in}}(x)}$, where $C^{\text{in}}(x)$ denotes the mean pixel value of the current view image $C^{\text{in}}(x)$, which better ensures the handling of input images with varying lighting conditions.

3.3.2. Curve-level Loss Constraints

Beyond image-level losses, we introduce curve-level loss constraints on \mathbb{L} to control both its values and shape, which is essential for generating pseudo-enhanced images C^{out} and for overall Luminance-GS training stability.

To prevent excessive divergence of the curve \mathbb{L} , we incorporate a shape regularization term that guides the curve to approximate specific patterns: the Power Curve \mathbb{L}_{po} , and the S-Curve \mathbb{L}_s , equation as follows. This regularization term serves as a prior, effectively restricting the curve’s shape and ensuring that the generated images remain smooth (see supplementary). Equation as follows:

$$\begin{aligned} \mathbb{L}_{po} : y &= (x + \epsilon)^{\mathbb{G}_k}, \epsilon = 1e^{-4} & 0 \leq x \leq 1 \\ \mathbb{L}_s : y &= \begin{cases} \mathbb{A}_k - \mathbb{A}_k \cdot \left(1 - \frac{x}{\mathbb{A}_k}\right)^{\mathbb{B}_k}, & \text{if } 0 \leq x \leq \mathbb{A}_k \\ \mathbb{A}_k + (1 - \mathbb{A}_k) \cdot \left(\frac{x - \mathbb{A}_k}{1 - \mathbb{A}_k}\right)^{\mathbb{B}_k}, & \text{if } 1 \geq x > \mathbb{A}_k \end{cases} \end{aligned} \quad (9)$$

where $\{\mathbb{G}_k, \mathbb{A}_k, \mathbb{B}_k\}$ are the view-adaptive learnable parameters, same as the view-adaptive curve generator, we additionally design another view-adaptive parameter generator to learn and predict $\{\mathbb{G}_k, \mathbb{A}_k, \mathbb{B}_k\}$ (see Fig. 4(c)). Additionally, to control curve value, we use cumulative distribution function (CDF) \mathbb{L}_{cdf} of the histogram-equalized (HE) input image $C^{\text{in}}(x)$ as the initial target values, the curve loss $\mathcal{L}_{\text{curve}}$ is set to learn both \mathbb{L}_{cdf} and shaped parameters:

$$\mathcal{L}_{\text{curve}} = \omega \|\mathbb{L} - \mathbb{L}_{\text{cdf}}\|^2 + 0.5 \|\mathbb{L} - (\mathbb{L}_{po} \cdot \mathbb{L}_s)\|^2 \quad (10)$$

where ω is a weight parameter, set to 1.0 for the first 3,000 iterations and set to 0.1 after 3,000 iterations, please refer to our supplementary for more details. Additionally, a total variation (TV) loss is incorporated between adjacent values in \mathcal{L} to enforce smoothness, defined as follows:

$$\mathcal{L}_{\text{tv}} = (1/255) \cdot \sum_{i \in (0, 254)} |\mathcal{L}(i+1) - \mathcal{L}(i)|^2 \quad (11)$$

Table 1. Mean results of LOM dataset [15] low-light subset (PSNR \uparrow , SSIM \uparrow , LPIPS \downarrow). Best results are bolded, second-best underlined, per-scene results please refer to supplementary.

Method	PSNR/ SSIM/ LPIPS	Method	PSNR/ SSIM/ LPIPS
GS [29]	6.88/ 0.157/ 0.662	GS + Z-DCE [23]	13.64/ 0.672/ 0.408
Z-DCE [23] + GS	13.45/ 0.702/ 0.349	GS + SCI [39]	15.22/ 0.748/ 0.430
SCI [39] + GS	11.73/ 0.692/ 0.407	GS + NeRCo [54]	17.21/ 0.712/ 0.421
NeRCo [54] + GS	17.59/ 0.727/ <u>0.345</u>	LLVE [61] + GS	16.43/ 0.728/ 0.399
SGZ [64] + GS	14.14/ 0.706/ 0.353	AME-NeRF [67]	17.65/ 0.729/ 0.405
Aleth-NeRF [15]	19.87/ <u>0.754</u>/ 0.417	Luminance-GS	<u>18.34/ 0.799/ 0.294</u>

Finally, the total loss of Luminance-GS is defined as:

$$\mathcal{L}_{\text{total}} = \mathcal{L}_{\text{reg}} + \mathcal{L}_{\text{spa}} + \mathcal{L}_{\text{tv}} + 10 \cdot \mathcal{L}_{\text{curve}}. \quad (12)$$

4. Experiments

Our code is based on open-source toolbox GS-Splat [58]. We evaluate our model under 3 different lighting conditions: (a) low-light, (b) overexposure, and (c) varying exposure. We present the dataset information and comparative methods, followed by experimental results and ablation details.

Dataset: For (a) low-light condition, we adopt low-light subset of the LOM dataset [15], which includes five scenes: “*buu*,” “*chair*,” “*sofa*,” “*bike*,” and “*shrub*.” Each scene provides low-light base views for training and normal-light novel views for evaluation. For (b) overexposure condition, we use the overexposure subset of the LOM dataset, which includes the same scenes but provides overexposed views for training and normal-light views for evaluation. For (c) varying exposure condition, we adopt unbounded Mip-NeRF 360 dataset [3], we synthesize each training views with different exposure conditions [1], meanwhile we also apply a slight gamma adjustment to each view to increase the difficulty (see Fig. 1 and Fig. 3 for examples). The unbounded 360° scene and varying exposure conditions would make NVS task more challenging.

Comparison Methods: For (a) low-light condition, we first compare with original 3DGS [29]. Then, we compare with combination of SOTA 2D image & video enhancement methods (Z-DCE [23], SCI [39], NeRCo [54], SGZ [64], LLVE [61]) with 3DGS, includes using enhancement methods to pre-process images for training (“+” + 3DGS in Table 1) and applying enhancement methods to post-processing images during rendering (3DGS + “+” in Table 1). Finally, we compare with two NeRF-based enhancement methods: AME-NeRF [67] and Aleth-NeRF [15].

For (b) overexposure condition, we compare with 3DGS [29], combination of 3DGS and 2D exposure correction methods (MSEC [1], IAT [14], MSLT [65], Adobe Lightroom[®] manually adjustment) and 3DGS, as well as NeRF-based exposure correction method Aleth-NeRF.

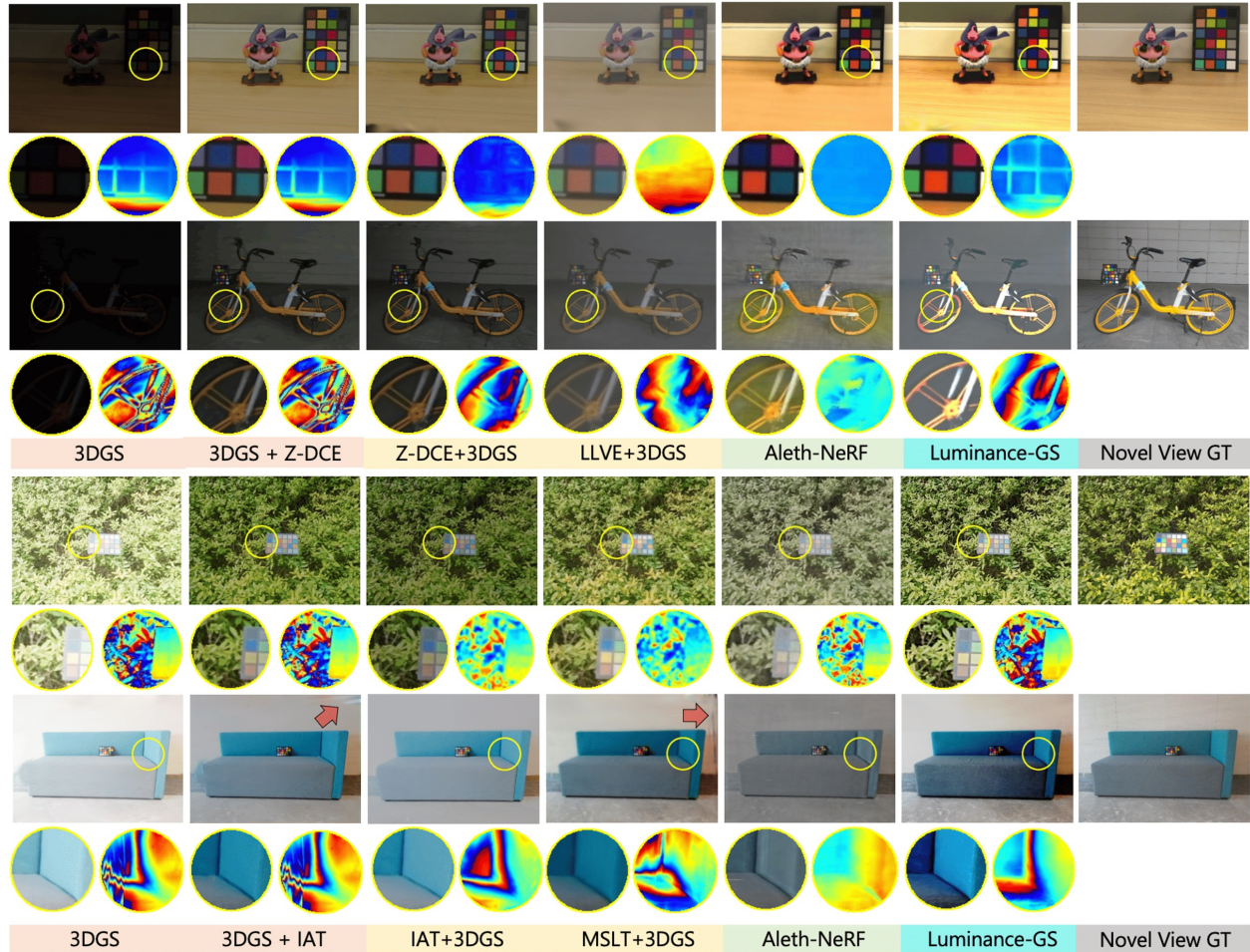


Figure 5. Novel view synthesis results on LOM dataset [15] low-light “*buu*”, “*bike*” scenes and overexposure “*shrub*”, “*sofa*” scenes.

For (c) varying exposure conditions, we compare with 3DGS [29], NeRF-based enhancement method Aleth-NeRF, NeRF-based in-the-wild method NeRF-W [40], and its recent 3DGS follow-up, GS-W [60]. Due to page limitation, we only show 3 scenes results “*bicycle*”, “*garden*” and “*counter*” here, full results please refer to supplementary.

4.1. Experimental Results

The (a) low-light experimental results is shown in Table. 1, we show the mean results of all 5 scenes ², with comparison of various methods, our Luminance-GS achieved the best results in both SSIM and LPIPS, outperforming the previous SOTA method [15] with an improvement of $\uparrow 0.44$ in SSIM and $\downarrow 0.123$ in LPIPS, although our PSNR is the second best, we achieve better detail recovery and more reliable depth maps (see Fig. 5). The (b) overexposure experimental results is shown in Table. 2, our Luminance-GS achieved the best results in all metrics, showing significant improvement over other methods. Fig. 1 showcases a com-

²Per scene results is shown in our supplementary part.

Table 2. Mean results of LOM dataset [15] overexposure subset. Best results are bolded, second-best underlined.

Method	PSNR/ SSIM/ LPIPS	Method	PSNR/ SSIM/ LPIPS
GS [29]	9.64/ 0.726/ 0.392	GS + MSEC [1]	19.56/ 0.805/ 0.382
MSEC [1] + GS	17.20/ 0.767/ 0.363	GS + IAT [14]	20.23/ 0.821/ 0.347
IAT [14] + GS	17.56/ 0.800/ 0.311	GS + MSLT [65]	<u>20.39</u> / 0.815/ 0.345
MSLT [65] + GS	20.25/ <u>0.824</u> / <u>0.262</u>	Lightroom + GS	19.91/ 0.785/ 0.308
Aleth-NeRF [15]	18.09/ 0.745/ 0.488	Luminance-GS	20.71/ 0.835/ 0.222

parison of efficiency. Some qualitative results can be found in Fig. 5, compared to other approaches, our Luminance-GS effectively preserves 3D multi-view consistency meanwhile retains rich details and vivid color appearance.

The (c) varying exposure experimental results are shown in Table 3. Our method achieves state-of-the-art (SOTA) image quality with rendering FPS on par with the original 3DGS [29], though with a slightly longer training time. The visualization results is shown in Fig. 6, we can find that

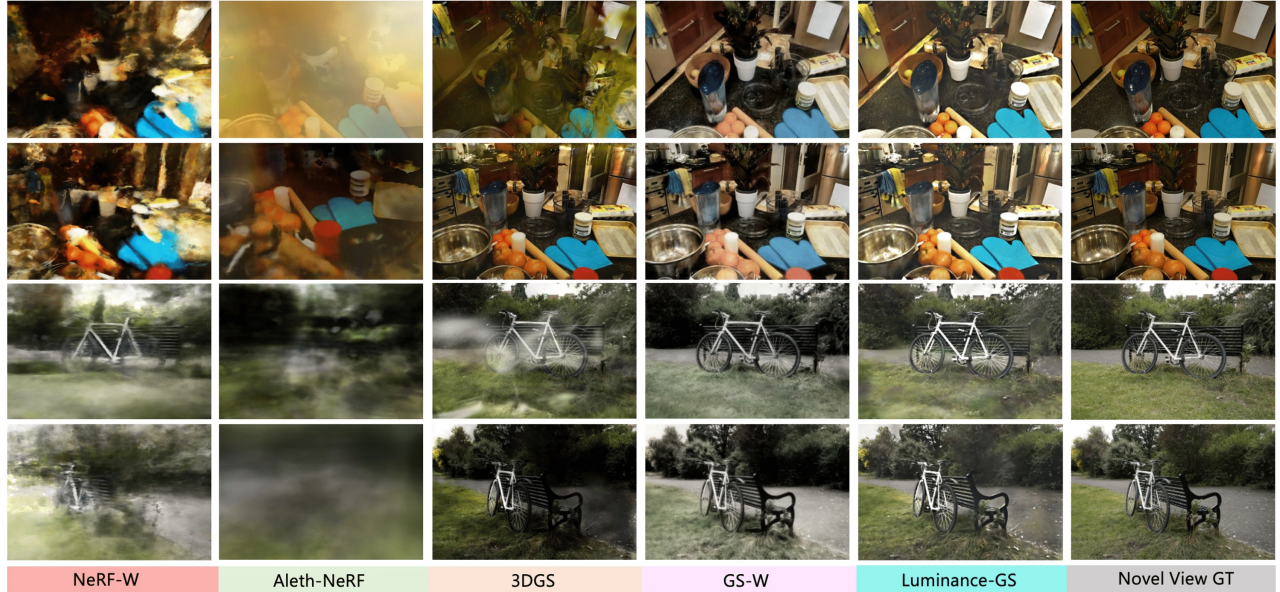


Figure 6. Novel view synthesis results on our synthesized varying exposure unbounded dataset (from Mip-NeRF 360 dataset [2]) “counter” and “bicycle” scenes, with comparison of NeRF-W [40], Aleth-NeRF [15], 3DGS [29] and GS-W [60].

Table 3. Comparison on varying exposure dataset, red color shows best result meanwhile yellow color shows second best result.

scene	metric	3DGS	NeRF-W	Aleth-NeRF	GS-W	Ours
“bicycle”	PSNR \uparrow	18.87	13.87	11.45	19.00	18.90
	SSIM \uparrow	0.618	0.231	0.154	0.603	0.640
	LPIPS \downarrow	0.333	0.603	0.772	0.356	0.302
“garden”	PSNR \uparrow	19.05	10.71	11.34	20.49	21.01
	SSIM \uparrow	0.731	0.222	0.245	0.765	0.786
	LPIPS \downarrow	0.242	0.687	0.758	0.222	0.219
“counter”	PSNR \uparrow	18.90	14.19	10.11	18.92	19.81
	SSIM \uparrow	0.670	0.319	0.187	0.677	0.698
	LPIPS \downarrow	0.276	0.641	0.745	0.328	0.271
GPU hrs \downarrow		~ 5min	~ 38hrs	~ 8hrs	~ 45min	~ 14min
FPS \uparrow		~ 150	0.138	0.875	~ 80	~ 150

Aleth-NeRF [15] and 3DGS [29] are unable to handle the variations in lighting and color, meanwhile NeRF-W [40] faces challenges in unbounded scenes. Finally, compared to GS-W [60], our method achieves better color recovery and results closer to the ground truth.

4.2. Ablation Analyze

We conducted additional ablation studies to verify the effectiveness of each module in our curve design, we analyze the different part of curve \mathbb{L} , and the results is shown in Table. 4, we performed experiments on scenes under three

Table 4. Ablation details of different parts in the curve design.

curve type	“buu” (low-light)	“buu” (overexposure)	“garden” (varying)
\mathbb{L}^g only	17.98/ 0.796/ 0.211	19.00/ 0.789/ 0.343	12.46/ 0.542/ 0.588
\mathbb{L}_k^b only	17.78/ 0.653/ 0.377	16.43/ 0.712/ 0.461	19.05/ 0.777/ 0.256
$\mathbb{L}^g + \mathbb{L}_k^b$	18.05/ 0.859/ 0.198	19.37/ 0.804/ 0.344	20.08/ 0.788 / 0.234
$\mathbb{L}^g + \mathbb{L}_k^b + \mathcal{M}_k$	18.09/ 0.877/ 0.193	19.67/ 0.811/ 0.311	21.01/ 0.786/ 0.219

different lighting conditions. From Table. 4 we can find that the global curve \mathbb{L}^g performs well in evenly lit environments (low-light, overexposure), meanwhile \mathbb{L}_k^b plays a key role in varying exposure scenarios, our approach of combining \mathbb{L}^g and \mathbb{L}_k^b leads to improvements across all lighting scenarios. Meanwhile, the design of the projection matrix \mathcal{M}_k has also proven effective in nearly all scenarios, demonstrating the effectiveness of per-view color matrix mapping. For more ablation analysis regarding the loss function, please refer to our supplementary material.

5. Conclusion

In this paper, we propose **Luminance-GS**, which improves the robustness of 3D Gaussian Splatting under challenging lighting conditions, such as low-light, overexposure, and varying exposure. Compared with previous methods, Luminance-GS offers superior illumination generalization and speed advantages, while achieving state-of-the-art (SOTA) performance on both real-world and synthetic datasets. In the future, we aim to extend our method to achieve scene generalization, enabling it to handle both illumination and scene variability.

6. Acknowledgment

This research is partially supported by JST Moonshot R&D Grant Number JPMJPS2011, CREST Grant Number JPMJCR2015 and Basic Research Grant (Super AI) of Institute for AI and Beyond of the University of Tokyo.

References

- [1] Mahmoud Afifi, Konstantinos G. Derpanis, Bjorn Ommer, and Michael S. Brown. Learning multi-scale photo exposure correction. In *Proceedings of the IEEE/CVF Conference on Computer Vision and Pattern Recognition (CVPR)*, pages 9157–9167, 2021. 1, 6, 7, 12, 14, 16
- [2] Jonathan T. Barron, Ben Mildenhall, Matthew Tancik, Peter Hedman, Ricardo Martin-Brualla, and Pratul P. Srinivasan. Mip-nerf: A multiscale representation for anti-aliasing neural radiance fields, 2021. 8, 17
- [3] Jonathan T. Barron, Ben Mildenhall, Dor Verbin, Pratul P. Srinivasan, and Peter Hedman. Mip-nerf 360: Unbounded anti-aliased neural radiance fields. *CVPR*, 2022. 1, 2, 6
- [4] Jonathan T. Barron, Ben Mildenhall, Dor Verbin, Pratul P. Srinivasan, and Peter Hedman. Zip-nerf: Anti-aliased grid-based neural radiance fields. *ICCV*, 2023. 1, 2
- [5] Vladimir Bychkovsky, Sylvain Paris, Eric Chan, and Fredo Durand. Learning photographic global tonal adjustment with a database of input / output image pairs. In *CVPR 2011*, pages 97–104, 2011. 2, 4
- [6] Yuanhao Cai, Yixun Liang, Jiahao Wang, Angtian Wang, Yulun Zhang, Xiaokang Yang, Zongwei Zhou, and Alan Yuille. Radiative gaussian splatting for efficient x-ray novel view synthesis. *arXiv preprint arXiv:2403.04116*, 2024. 2
- [7] Yuanhao Cai, Zihao Xiao, Yixun Liang, Yulun Zhang, Xiaokang Yang, Yaoyao Liu, and Alan Yuille. Hdr-gs: Efficient high dynamic range novel view synthesis at 1000x speed via gaussian splatting. *arXiv preprint arXiv:2405.15125*, 2024. 2
- [8] Nicolas Carion, Francisco Massa, Gabriel Synnaeve, Nicolas Usunier, Alexander Kirillov, and Sergey Zagoruyko. End-to-end object detection with transformers. In *Computer Vision – ECCV 2020*, pages 213–229, Cham, 2020. Springer International Publishing. 5
- [9] Cheng-Kang Ted Chao, Jason Klein, Jianchao Tan, Jose Echevarria, and Yotam Gingold. Colorfulcurves: Palette-aware lightness control and color editing via sparse optimization. *ACM Trans. Graph.*, 42(4), 2023. 3
- [10] David Charatan, Sizhe Li, Andrea Tagliasacchi, and Vincent Sitzmann. pixelsplat: 3d gaussian splats from image pairs for scalable generalizable 3d reconstruction. In *arXiv*, 2023. 1, 2
- [11] Xingyu Chen, Qi Zhang, Xiaoyu Li, Yue Chen, Ying Feng, Xuan Wang, and Jue Wang. Hallucinated neural radiance fields in the wild. In *Proceedings of the IEEE/CVF Conference on Computer Vision and Pattern Recognition*, pages 12943–12952, 2022. 2, 3
- [12] Yuedong Chen, Haofei Xu, Chuanxia Zheng, Bohan Zhuang, Marc Pollefeys, Andreas Geiger, Tat-Jen Cham, and Jianfei Cai. Mvsplat: Efficient 3d gaussian splatting from sparse multi-view images. *arXiv preprint arXiv:2403.14627*, 2024. 2
- [13] Ilya Chugunov, Amogh Joshi, Kiran Murthy, Francois Bleibel, and Felix Heide. Neural light spheres for Implicit Image Stitching and View Synthesis. In *Proceedings of the ACM SIGGRAPH Asia 2024*. ACM, 2024. 2
- [14] Ziteng Cui, Kunchang Li, Lin Gu, Shenghan Su, Peng Gao, ZhengKai Jiang, Yu Qiao, and Tatsuya Harada. You only need 90k parameters to adapt light: a light weight transformer for image enhancement and exposure correction. In *33rd British Machine Vision Conference 2022, BMVC 2022, London, UK, November 21-24, 2022*. BMVA Press, 2022. 1, 5, 6, 7, 14, 16
- [15] Ziteng Cui, Lin Gu, Xiao Sun, Xianzheng Ma, Yu Qiao, and Tatsuya Harada. Aleth-nerf: Illumination adaptive nerf with concealing field assumption. In *Proceedings of the AAAI Conference on Artificial Intelligence*, 2024. 1, 2, 3, 6, 7, 8, 12, 14, 15, 16, 17
- [16] Ziteng Cui, Lin Gu, and Tatsuya Harada. Discovering an image-adaptive coordinate system for photography processing. *arXiv preprint arXiv:2501.06448*, 2025. 3, 5
- [17] Hiba Dahmani, Moussab Bennehar, Nathan Piasco, Luis Roldão, and Dzmitry V. Tsishkou. Swag: Splatting in the wild images with appearance-conditioned gaussians. *ArXiv*, abs/2403.10427, 2024. 3
- [18] Kangle Deng, Andrew Liu, Jun-Yan Zhu, and Deva Ramanan. Depth-supervised NeRF: Fewer views and faster training for free. In *Proceedings of the IEEE/CVF Conference on Computer Vision and Pattern Recognition (CVPR)*, 2022. 1, 2
- [19] Alexey Dosovitskiy, Lucas Beyer, Alexander Kolesnikov, Dirk Weissenborn, Xiaohua Zhai, Thomas Unterthiner, Mostafa Dehghani, Matthias Minderer, Georg Heigold, Sylvain Gelly, Jakob Uszkoreit, and Neil Houlsby. An image is worth 16x16 words: Transformers for image recognition at scale. In *International Conference on Learning Representations*, 2021. 5
- [20] Zhiwen Fan, Kevin Wang, Kairun Wen, Zehao Zhu, Dejia Xu, and Zhangyang Wang. Lightgaussian: Unbounded 3d gaussian compression with 15x reduction and 200+ fps, 2023. 2
- [21] Yang Fu, Sifei Liu, Amey Kulkarni, Jan Kautz, Alexei A. Efros, and Xiaocong Wang. Colmap-free 3d gaussian splatting. In *Proceedings of the IEEE/CVF Conference on Computer Vision and Pattern Recognition (CVPR)*, pages 20796–20805, 2024. 2
- [22] Antoine Guédon and Vincent Lepetit. Sugar: Surface-aligned gaussian splatting for efficient 3d mesh reconstruction and high-quality mesh rendering. *CVPR*, 2024. 2
- [23] Chunle Guo, Chongyi Li, Jichang Guo, Chen Change Loy, Junhui Hou, Sam Kwong, and Runmin Cong. Zero-reference deep curve estimation for low-light image enhancement. In *Proceedings of the IEEE conference on computer vision and pattern recognition (CVPR)*, pages 1780–1789, 2020. 1, 3, 6, 14
- [24] Wang Haoyuan, Xu Xiaogang, Xu Ke, and W.H. Lau Rynson. Lighting up nerf via unsupervised decomposition and enhancement. In *ICCV*, 2023. 1, 2, 3

- [25] Binbin Huang, Zehao Yu, Anpei Chen, Andreas Geiger, and Shenghua Gao. 2d gaussian splatting for geometrically accurate radiance fields. In *SIGGRAPH 2024 Conference Papers*. Association for Computing Machinery, 2024. 2
- [26] Ting Jiang, Chuan Wang, Xinpeng Li, Ru Li, Haoqiang Fan, and Shuaicheng Liu. Meflut: Unsupervised 1d lookup tables for multi-exposure image fusion. In *Proceedings of the IEEE/CVF International Conference on Computer Vision*, pages 10542–10551, 2023. 3
- [27] Xin Jin, Pengyi Jiao, Zheng-Peng Duan, Xingchao Yang, Chun-Le Guo, Bo Ren, and Chong-Yi Li. Lighting every darkness with 3dgs: Fast training and real-time rendering for hdr view synthesis. In *arxiv preprint*, 2024. 3
- [28] Sing Bing Kang, Ashish Kapoor, and Dani Lischinski. Personalization of image enhancement. In *2010 IEEE Computer Society Conference on Computer Vision and Pattern Recognition*, pages 1799–1806, 2010. 2
- [29] Bernhard Kerbl, Georgios Kopanas, Thomas Leimkühler, and George Drettakis. 3d gaussian splatting for real-time radiance field rendering. *ACM Transactions on Graphics*, 42(4), 2023. 1, 2, 3, 6, 7, 8, 12, 14, 15, 16, 17
- [30] Shakiba Kheradmand, Daniel Rebain, Gopal Sharma, Weiwei Sun, Jeff Tseng, Hossam Isack, Abhishek Kar, Andrea Tagliasacchi, and Kwang Moo Yi. 3d gaussian splatting as markov chain monte carlo. *arXiv preprint arXiv:2404.09591*, 2024. 2
- [31] Han-Ul Kim, Young Jun Koh, and Chang-Su Kim. Global and local enhancement networks for paired and unpaired image enhancement. In *Computer Vision – ECCV 2020*, pages 339–354, Cham, 2020. Springer International Publishing. 3
- [32] Jonas Kulhanek, Songyou Peng, Zuzana Kukelova, Marc Pollefeys, and Torsten Sattler. WildGaussians: 3D gaussian splatting in the wild. *arXiv*, 2024. 2, 3, 5
- [33] Hyeongmin Lee, Kyoungkook Kang, Jungseul Ok, and Sunghyun Cho. Cliptone: Unsupervised learning for text-based image tone adjustment. In *Proceedings of the IEEE/CVF Conference on Computer Vision and Pattern Recognition*, pages 2942–2951, 2024. 3
- [34] Ruilong Li, Hang Gao, Matthew Tancik, and Angjoo Kanazawa. Nerfacc: Efficient sampling accelerates nerfs. In *Proceedings of the IEEE/CVF International Conference on Computer Vision (ICCV)*, pages 18537–18546, 2023. 1, 2
- [35] Ruilong Li, Sanja Fidler, Angjoo Kanazawa, and Francis Williams. NeRF-XL: Scaling nerfs with multiple GPUs. In *European Conference on Computer Vision (ECCV)*, 2024. 1, 2
- [36] Zhihao Li, Yufei Wang, Alex Kot, and Bihan Wen. From chaos to clarity: 3dgs in the dark, 2024. 3
- [37] Zhihao Liang, Qi Zhang, Ying Feng, Ying Shan, and Kui Jia. Gs-ir: 3d gaussian splatting for inverse rendering. In *Proceedings of the IEEE/CVF Conference on Computer Vision and Pattern Recognition*, pages 21644–21653, 2024. 1, 2
- [38] Tianqi Liu, Guangcong Wang, Shoukang Hu, Liao Shen, Xinyi Ye, Yuhang Zang, Zhiguo Cao, Wei Li, and Ziwei Liu. Mvsgaussian: Fast generalizable gaussian splatting reconstruction from multi-view stereo. In *European Conference on Computer Vision*, pages 37–53. Springer, 2025. 1, 2
- [39] Long Ma, Tengyu Ma, Risheng Liu, Xin Fan, and Zhongxuan Luo. Toward fast, flexible, and robust low-light image enhancement. In *Proceedings of the IEEE/CVF Conference on Computer Vision and Pattern Recognition*, pages 5637–5646, 2022. 1, 6, 14, 15
- [40] Ricardo Martin-Brualla, Noha Radwan, Mehdi S. M. Sajjadi, Jonathan T. Barron, Alexey Dosovitskiy, and Daniel Duckworth. NeRF in the Wild: Neural Radiance Fields for Unconstrained Photo Collections. In *CVPR*, 2021. 2, 3, 7, 8, 17
- [41] Ben Mildenhall, Pratul P. Srinivasan, Matthew Tancik, Jonathan T. Barron, Ravi Ramamoorthi, and Ren Ng. Nerf: Representing scenes as neural radiance fields for view synthesis. In *ECCV*, 2020. 1, 2
- [42] Ben Mildenhall, Peter Hedman, Ricardo Martin-Brualla, Pratul P. Srinivasan, and Jonathan T. Barron. NeRF in the dark: High dynamic range view synthesis from noisy raw images. *arXiv*, 2021. 1, 3
- [43] Sean Moran, Steven McDonagh, and Gregory Slabaugh. Curl: Neural curve layers for global image enhancement. In *2020 25th International Conference on Pattern Recognition (ICPR)*, pages 9796–9803, 2021. 3
- [44] Simon Niedermayr, Josef Stumpfegger, and Rüdiger Westermann. Compressed 3d gaussian splatting for accelerated novel view synthesis. In *Proceedings of the IEEE/CVF Conference on Computer Vision and Pattern Recognition (CVPR)*, pages 10349–10358, 2024. 1
- [45] Zefan Qu, Ke Xu, Gerhard Petrus Hancke, and Rynson W. H. Lau. Lush-nerf: Lighting up and sharpening nerfs for low-light scenes. In *The Thirty-eighth Annual Conference on Neural Information Processing Systems*, 2024. 3
- [46] Erik Reinhard, Michael Stark, Peter Shirley, and James Ferwerda. Photographic tone reproduction for digital images. *ACM Trans. Graph.*, 21(3):267–276, 2002. 2
- [47] Viktor Rudnev, Mohamed Elgharib, William Smith, Lingjie Liu, Vladislav Golyanik, and Christian Theobalt. Nerf for outdoor scene relighting. In *European Conference on Computer Vision (ECCV)*, 2022. 1
- [48] David Serrano-Lozano, Luis Herranz, Michael S. Brown, and Javier Vazquez-Corral. Colorcurves: Learned image enhancement via color naming. *ECCV*, 2024. 3, 4
- [49] Shreyas Singh, Aryan Garg, and Kaushik Mitra. Hdrsplat: Gaussian splatting for high dynamic range 3d scene reconstruction from raw images. *BMVC*, 2024. 3
- [50] Stanislaw Szymanowicz, Christian Rupprecht, and Andrea Vedaldi. Splatter image: Ultra-fast single-view 3d reconstruction. In *The IEEE/CVF Conference on Computer Vision and Pattern Recognition (CVPR)*, 2024. 2
- [51] Wenjing Wang, Zhengbo Xu, Haofeng Huang, and Jiaying Liu. Self-aligned concave curve: Illumination enhancement for unsupervised adaptation. In *Proceedings of the ACM International Conference on Multimedia*, 2022. 3
- [52] Yuehao Wang, Chaoyi Wang, Bingchen Gong, and Tianfan Xue. Bilateral guided radiance field processing. *ACM Transactions on Graphics (TOG)*, 43(4):1–13, 2024. 1, 2, 3
- [53] Jiacong Xu, Mingqian Liao, K Ram Prabhakar, and Vishal M Patel. Leveraging thermal modality to en-

- hance reconstruction in low-light conditions. *arXiv preprint arXiv:2403.14053*, 2024. 3
- [54] Shuzhou Yang, Moxuan Ding, Yanmin Wu, Zihan Li, and Jian Zhang. Implicit neural representation for cooperative low-light image enhancement. In *Proceedings of the IEEE/CVF International Conference on Computer Vision (ICCV)*, pages 12918–12927, 2023. 6, 14
- [55] Shuzhou Yang, Xuanyu Zhang, Yinhuai Wang, Jiwen Yu, Yuhan Wang, and Jian Zhang. Diffle: Diffusion-guided domain calibration for unsupervised low-light image enhancement, 2023. 3
- [56] Yifan Yang, Shuhai Zhang, Zixiong Huang, Yubing Zhang, and Mingkui Tan. Cross-ray neural radiance fields for novel-view synthesis from unconstrained image collections. In *Proceedings of the IEEE/CVF International Conference on Computer Vision*, pages 15901–15911, 2023. 2, 3
- [57] Sheng Ye, Zhen-Hui Dong, Yubin Hu, Yu-Hui Wen, and Yong-Jin Liu. Gaussian in the dark: Real-time view synthesis from inconsistent dark images using gaussian splatting. *arXiv preprint arXiv:2408.09130*, 2024. 3
- [58] Vickie Ye, Ruilong Li, Justin Kerr, Matias Turkulainen, Brent Yi, Zhuoyang Pan, Otto Seiskari, Jianbo Ye, Jeffrey Hu, Matthew Tancik, and Angjoo Kanazawa. gsplat: An open-source library for Gaussian splatting. *arXiv preprint arXiv:2409.06765*, 2024. 6, 12
- [59] Lu Yuan and Jian Sun. Automatic exposure correction of consumer photographs. In *European Conference on Computer Vision*, 2012. 2, 4
- [60] Dongbin Zhang, Chuming Wang, Weitao Wang, Peihao Li, Minghan Qin, and Haoqian Wang. Gaussian in the wild: 3d gaussian splatting for unconstrained image collections. *ECCV*, 2024. 1, 2, 3, 5, 7, 8, 17
- [61] Fan Zhang, Yu Li, Shaodi You, and Ying Fu. Learning temporal consistency for low light video enhancement from single images. In *Proceedings of the IEEE/CVF Conference on Computer Vision and Pattern Recognition (CVPR)*, pages 4967–4976, 2021. 6, 14
- [62] Kai Zhang, Gernot Riegler, Noah Snavely, and Vladlen Koltun. Nerf++: Analyzing and improving neural radiance fields. *arXiv:2010.07492*, 2020. 1
- [63] Tianyi Zhang, Kaining Huang, Weiming Zhi, and Matthew Johnson-Roberson. Darkgs: Learning neural illumination and 3d gaussians relighting for robotic exploration in the dark. *2024 International Conference on Intelligent Robots and Systems (IROS)*, 2024. 3
- [64] Shen Zheng and Gaurav Gupta. Semantic-guided zero-shot learning for low-light image/video enhancement. In *Proceedings of the IEEE/CVF Winter Conference on Applications of Computer Vision*, pages 581–590, 2022. 6, 14, 15
- [65] Yijie Zhou, Chao Li, Jin Liang, Tianyi Xu, Xin Liu, and Jun Xu. 4k-resolution photo exposure correction at 125 fps with 8k parameters. In *Winter Conference on Applications of Computer Vision (WACV)*, 2024. 6, 7, 14
- [66] Chengxuan Zhu, Renjie Wan, and Boxin Shi. Neural transmitted radiance fields. In *Advances in Neural Information Processing Systems*, pages 38994–39006. Curran Associates, Inc., 2022. 2
- [67] Yang Zou, Xingyuan Li, Zhiying Jiang, and Jinyuan Liu. Enhancing neural radiance fields with adaptive multi-exposure fusion: A bilevel optimization approach for novel view synthesis. In *Proceedings of the AAAI Conference on Artificial Intelligence*, pages 7882–7890, 2024. 1, 2, 3, 6, 14
- [68] Matthias Zwicker, Hanspeter Pfister, Jeroen Van Baar, and Markus Gross. Surface splatting. In *Proceedings of the 28th annual conference on Computer graphics and interactive techniques*, pages 371–378, 2001. 3



Figure 7. The limitation of our method, in some cases, Luminance-GS fails to correctly render colors, resulting in color discrepancies in certain areas and the occurrence of pixelation.

7. Detailed Experimental Results

Due to page limitations, we could not fully present the per-scene experimental results in the main text. Instead, we provide the complete experimental results in the supplementary part: the per-scene results for the LOM dataset low-light scene are shown in Table. 6, it can be observed that our method achieves excellent performance in most scenarios. Additionally, we found that Aleth-NeRF [15] is sensitive to hyper-parameter, for instance, if the enhance degree of Aleth-NeRF is set to a slightly lower value (e.g., reduced from 0.45 to 0.4), its PSNR value significantly decreases as well (see Table. 6). The results for overexposure scenes in the LOM dataset are presented in Table. 7, and the other 4 scenes results for our synthesized varying exposure dataset are shown in Table. 5. We can see that our Luminance-GS both achieves SOTA performance in PSNR, SSIM and LPIPS.

More visualization results are shown in Fig. 9, Fig. 10 and Fig. 11, we can found that sometimes image restoration modules easily lead to multi-view inconsistency, which ultimately causes floaters during rendering (see Fig. 10 “MSEC [1] + 3DGS” for example). Meanwhile, our method achieves better detail reconstruction results compared to other approaches. We have zoomed in on random areas to enlarge the details and demonstrate the superior performance of our detail recovery.

8. Ablation Analysis of Loss Functions

We further assess the effectiveness of various loss functions in our Luminance-GS model. Figure 8 illustrates this through the “sofa” scene, showcasing examples under both low-light and overexposure conditions.

From Fig. 8, we can find that spatial loss \mathcal{L}_{spa} (Eq.8 in main text) plays a crucial role in maintaining multi-view consistency, after removing loss \mathcal{L}_{spa} , the rendered scenes tend to exhibit large areas of floaters, which become partic-

Table 5. Other 4 scenes results on varying exposure unbounded dataset, we show the PSNR \uparrow , SSIM \uparrow and LPIPS \downarrow . Red indicates the best result, while blue indicates the second-best result.

Methods	“bonsai”	“kitchen”	“room”	“stump”
3DGS	19.05/ 0.699/ 0.403	18.54/ 0.703/ 0.398	19.66/ 0.812/ 0.356	18.12/ 0.698/ 0.366
NeRF-W	14.11/ 0.529/ 0.633	12.87/ 0.451/ 0.502	13.09/ 0.355/ 0.498	14.11/ 0.495/ 0.688
Aleth-NeRF	10.09/ 0.377/ 0.709	9.58/ 0.410/ 0.698	7.22/ 0.308/ 0.742	10.51/ 0.365/ 0.703
GS-W	19.78/ 0.698/ 0.363	18.55/ 0.722/ 0.369	19.32/ 0.794/ 0.386	18.35/ 0.721/ 0.350
Ours	19.77/ 0.709/ 0.351	18.47/ 0.751/ 0.348	20.44/ 0.811/ 0.331	18.64/ 0.732/ 0.344

ularly pronounced under low-light conditions. Meanwhile, in curve loss \mathcal{L}_{curve} (Eq.10 in main text), the cumulative distribution function (CDF) \mathbb{L}_{cdf} of the histogram-equalized (HE) $C^{in}(x)$ is essential for controlling the degree of illumination. Without \mathbb{L}_{cdf} , efforts to enhance or attenuate illumination are often unsuccessful. Additionally, the pre-defined curve shape $\mathbb{L}_{po} \cdot \mathbb{L}_s$ (Eq.9 in main text) maintain the smoothness of the generated images, reducing the likelihood of large areas of pixels collapsing into a single value, ensuring the generated images more aligned with human visual perception. Ultimately, with the assistance of all the aforementioned losses, we can achieve satisfactory rendered novel views, as shown in the last column of Fig. 8.

9. Experimental Setup

For training settings, we trained Luminance-GS on a single Nvidia Tesla V100 GPU using the Adam optimizer. The learning rates for the various parameters were set as follows:

- For the basic 3DGS parameters $G_i = \{\mu_i, c_i, o_i, \Sigma_i\}$, we adopted the default settings from GS-Splat [58].
- The learning rates for the color adjustment parameters \mathbf{a}_i and \mathbf{b}_i were set to 2.5×10^{-3} .
- The learning rate for the color space mapping matrix \mathcal{M}_k was set to 2.5×10^{-4} , with a weight decay of 1×10^{-5} .
- The global curve \mathbb{L}^g was optimized with a learning rate of 1×10^{-3} and a weight decay of 1×10^{-4} .
- The learning rates for the two attention blocks (view-adaptive curve generator and view-adaptive parameters generator, as shown in Fig. 4 of the main text) were set to 1×10^{-5} , with a weight decay of 1×10^{-5} .

Training was conducted for a total of 10,000 iterations, with Gaussian refinement stopping at 8,000 iterations. For other settings, such as Gaussian reset steps [29], we adhered to the default configuration provided by GS-Splat [58].

10. Limitation and Future Discussion

Some failure cases are shown in Fig. 7. In certain scenes, Luminance-GS may lose fine details, such as the leaves of plants disappearing (see Fig. 7 above). Additionally, Luminance-GS sometimes renders incorrect colors and can exhibit pixelated artifacts, as seen in the chair’s color in

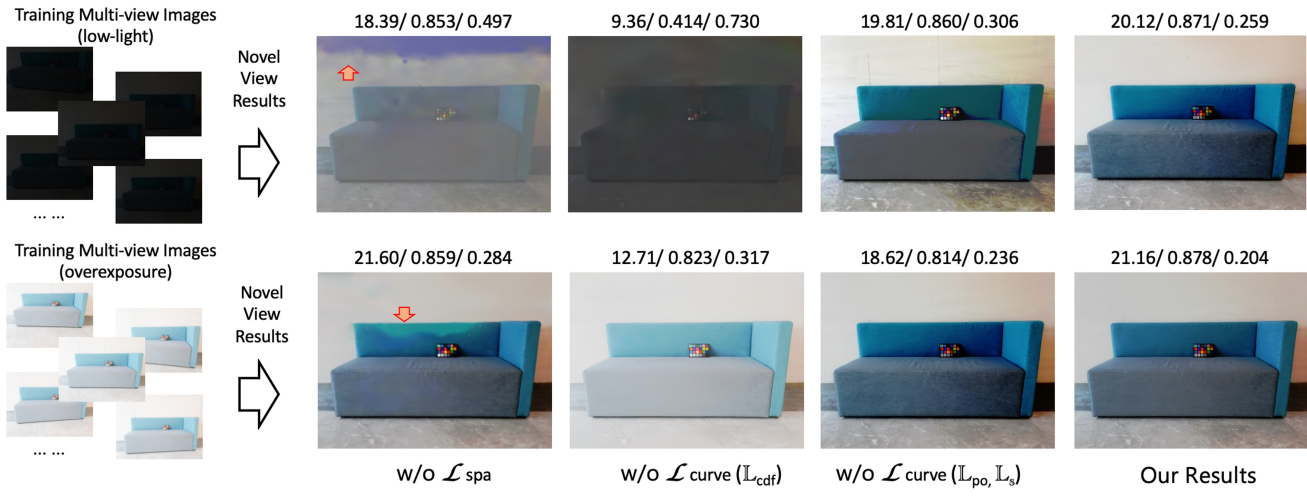


Figure 8. Ablation analysis of different loss functions in Luminance-GS, we denote PSNR \uparrow / SSIM \uparrow / LPIPS \downarrow value upon the figures.

Fig. 7 below. This could be due to errors in the pseudo-labels generated by curve \mathbb{L} , and we hope that future research can optimize both the training strategy and the pseudo-label generation solution.

For future research directions, we think that it would be valuable to consider more scenarios of internal camera degradation, such as inconsistent white balance settings. Exploring how to enable scene generalization with Luminance-GS is also a promising direction. Additionally, we believe that extending Luminance-GS to real-world applications, such as autonomous driving and underground coal mining scenarios, would be highly meaningful.

Table 6. Per-scene experimental results (PSNR \uparrow , SSIM \uparrow , LPIPS \downarrow) on LOM dataset [15] low-light subset, we compare with various enhancement methods [23, 39, 54, 61, 64] and NeRF-based methods [15, 67]. (*: The results of work [67] are directly taken from their paper). Red indicates the best result, while blue indicates the second-best result.

Method	“ <i>buu</i> ”	“ <i>chair</i> ”	“ <i>sofa</i> ”	“ <i>bike</i> ”	“ <i>shrub</i> ”	<i>mean</i>
	PSNR/ SSIM/ LPIPS	PSNR/ SSIM/ LPIPS	PSNR/ SSIM/ LPIPS	PSNR/ SSIM/ LPIPS	PSNR/ SSIM/ LPIPS	PSNR/ SSIM/ LPIPS
3DGS [29]	7.53/ 0.299/ 0.442	6.06/ 0.151/ 0.742	6.31/ 0.216/ 0.723	6.37/ 0.077/ 0.781	8.15/ 0.044/ 0.620	6.88/ 0.157/ 0.662
Image Enhancement Methods + 3DGS						
3DGS + Z-DCE [23]	18.02/ 0.834/ 0.303	12.55/ 0.725/ 0.478	14.66/ 0.822/ 0.460	10.26/ 0.509/ 0.491	12.93/ 0.468/ 0.309	13.64/ 0.672/ 0.408
Z-DCE [23] + 3DGS	17.83/ 0.874 / 0.350	12.47/ 0.762/ 0.399	13.86/ 0.841/ 0.308	10.37/ 0.544/ 0.441	12.74/ 0.487/ 0.248	13.45/ 0.702/ 0.349
3DGS + SCI [39]	13.80/ 0.845/ 0.339	19.70/ 0.812/ 0.455	19.63 / 0.851/ 0.455	12.86/ 0.621/ 0.463	16.14/ 0.600/ 0.442	15.22/ 0.748/ 0.430
SCI [39] + 3DGS	7.68/ 0.690/ 0.523	11.69/ 0.794/ 0.419	10.02/ 0.770/ 0.365	13.55/ 0.667/ 0.390	15.72/ 0.538/ 0.339	11.73/ 0.692/ 0.407
3DGS + NeRCo [54]	16.64/ 0.765/ 0.401	19.24/ 0.759/ 0.466	16.77/ 0.834/ 0.399	16.33/ 0.700/ 0.427	17.07/ 0.503/ 0.411	17.21/ 0.712/ 0.421
NeRCo [54] + 3DGS	16.69/ 0.802/ 0.330	19.11/ 0.773/ 0.376	18.04/ 0.868 / 0.381	16.16/ 0.703/ 0.397	17.97 / 0.502/ 0.399	17.59/ 0.727/ 0.345
Video Enhancement Methods + 3DGS						
LLVE [61] + 3DGS	19.67/ 0.868/ 0.253	15.29/ 0.805/ 0.424	17.18/ 0.858/ 0.379	14.01/ 0.677/ 0.452	15.98/ 0.430/ 0.488	16.43/ 0.728/ 0.399
SGZ [64] + 3DGS	19.21/ 0.832/ 0.270	12.30/ 0.755/ 0.377	14.54/ 0.815/ 0.329	10.61/ 0.563/ 0.375	14.04/ 0.565 / 0.416	14.14/ 0.706/ 0.353
NeRF-based Enhancement Methods						
AME-NeRF* [67]	19.89 / 0.854/ 0.312	17.05/ 0.751/ 0.381	17.93/ 0.847/ 0.378	18.14/ 0.732 / 0.437	15.23/ 0.462/ 0.518	17.65/ 0.729/ 0.405
Aleth-NeRF [15](0.45)	20.22 / 0.859/ 0.315	20.93 / 0.818 / 0.468	19.52/ 0.857/ 0.354	20.46 / 0.727/ 0.499	18.24 / 0.511/ 0.448	19.87 / 0.754 / 0.417
Aleth-NeRF [15](0.4)	19.14/ 0.839/ 0.306	16.96/ 0.793/ 0.483	16.97/ 0.847/ 0.367	17.56/ 0.719/ 0.468	17.55/ 0.484/ 0.451	17.64/ 0.736/ 0.415
Our Proposed Method						
Luminance-GS	18.09/ 0.877 / 0.193	19.82 / 0.835 / 0.367	20.12 / 0.871 / 0.259	18.27 / 0.749 / 0.411	15.40/ 0.666 / 0.241	18.34 / 0.799 / 0.294

Table 7. Per-scene experimental results (PSNR \uparrow , SSIM \uparrow , LPIPS \downarrow) on LOM dataset [15] overexposure scene, we compare with exposure correction methods [1, 14, 65] and NeRF-based methods [15]. Red indicates the best result, while blue indicates the second-best result.

Method	“ <i>buu</i> ”	“ <i>chair</i> ”	“ <i>sofa</i> ”	“ <i>bike</i> ”	“ <i>shrub</i> ”	<i>mean</i>
	PSNR/ SSIM/ LPIPS	PSNR/ SSIM/ LPIPS	PSNR/ SSIM/ LPIPS	PSNR/ SSIM/ LPIPS	PSNR/ SSIM/ LPIPS	PSNR/ SSIM/ LPIPS
3DGS [29]	6.96/ 0.674/ 0.609	11.14/ 0.790/ 0.362	10.17/ 0.790/ 0.369	9.58/ 0.730/ 0.323	10.34/ 0.646/ 0.299	9.64/ 0.726/ 0.392
Exposure Correction Methods + 3DGS						
3DGS + MSEC [1]	16.03/ 0.806 / 0.517	20.81/ 0.851 / 0.408	20.65/ 0.862/ 0.397	22.10/ 0.826/ 0.305	18.21/ 0.678/ 0.289	19.56/ 0.805/ 0.382
MSEC [1] + 3DGS	15.08/ 0.804/ 0.440	16.63/ 0.797/ 0.416	20.09/ 0.828/ 0.335	17.57/ 0.739/ 0.368	16.61/ 0.666/ 0.255	17.20/ 0.767/ 0.363
3DGS + IAT [14]	15.34/ 0.804/ 0.522	21.96 / 0.833/ 0.292	20.23/ 0.872 / 0.402	22.36/ 0.832/ 0.291	21.24 / 0.765/ 0.226	20.23/ 0.821/ 0.347
IAT [14] + 3DGS	15.86/ 0.803/ 0.387	18.61/ 0.830/ 0.367	17.42/ 0.833/ 0.348	19.17/ 0.801/ 0.235	16.74/ 0.731/ 0.219	17.56/ 0.800/ 0.311
3DGS + MSLT [65]	15.34/ 0.798/ 0.473	21.69/ 0.823/ 0.304	23.05 / 0.830/ 0.317	23.37/ 0.830/ 0.317	18.89 / 0.779/ 0.214	20.39 / 0.815/ 0.345
MSLT [65] + 3DGS	16.35/ 0.805/ 0.333	20.93/ 0.828/ 0.275	21.65 / 0.847/ 0.259	24.03 / 0.841 / 0.244	18.29/ 0.797 / 0.199	20.25/ 0.824 / 0.262
NeRF-based Exposure Correction Method						
Aleth-NeRF [15]	16.78 / 0.805/ 0.611	20.08/ 0.820/ 0.499	17.85/ 0.852/ 0.458	19.85/ 0.773/ 0.392	15.91/ 0.477/ 0.483	18.09/ 0.745/ 0.488
Our Proposed Method						
Luminance-GS	19.67 / 0.811 / 0.311	22.63 / 0.856 / 0.207	21.16/ 0.878 / 0.204	24.05 / 0.851 / 0.216	16.04/ 0.780 / 0.173	20.71 / 0.835 / 0.222

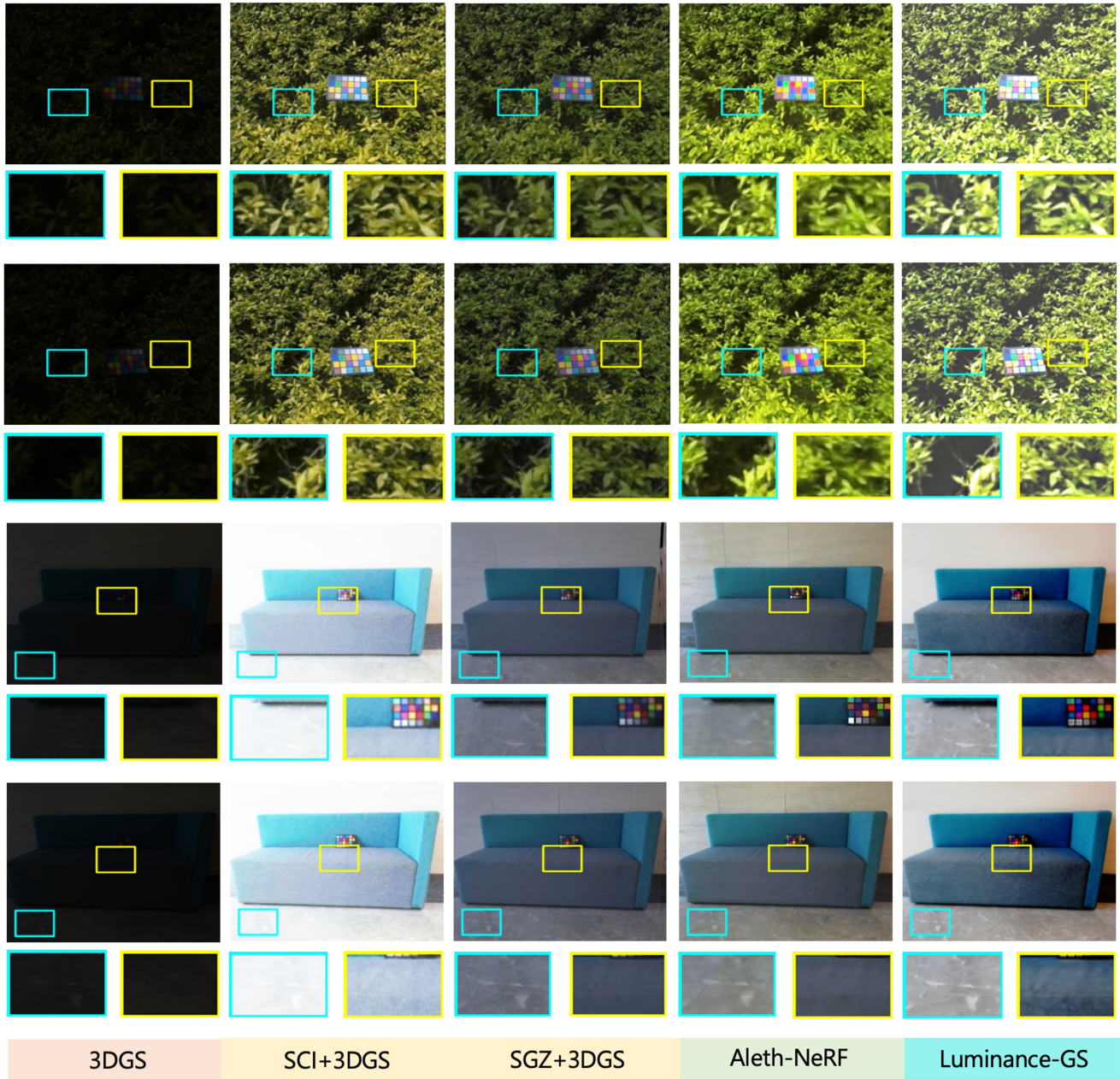


Figure 9. Novel view synthesis results in LOM dataset low-light “*shrub*” and “*sofa*” scenes, we show the comparison results with 3DGS [29], combination of low-light enhancement methods (SCI [39], SGZ [64]) with 3DGS and Aleth-NeRF [15].

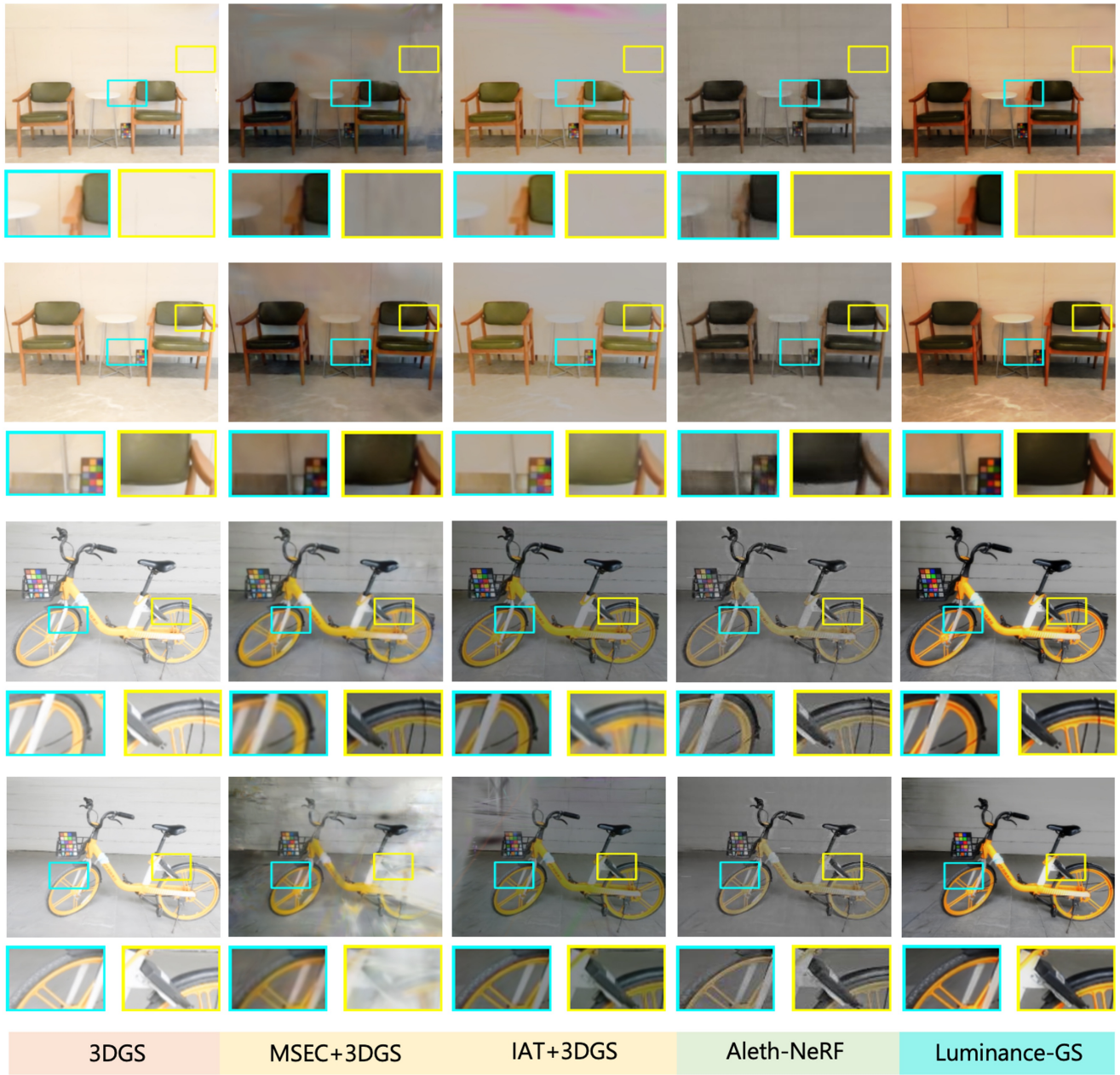


Figure 10. Novel view synthesis results in LOM dataset over-exposure “*chair*” and “*bike*” scenes, we show the comparison results with 3DGS [29], combination of exposure correction methods (MSEC [1], IAT [14]) with 3DGS and Aleth-NeRF [15].

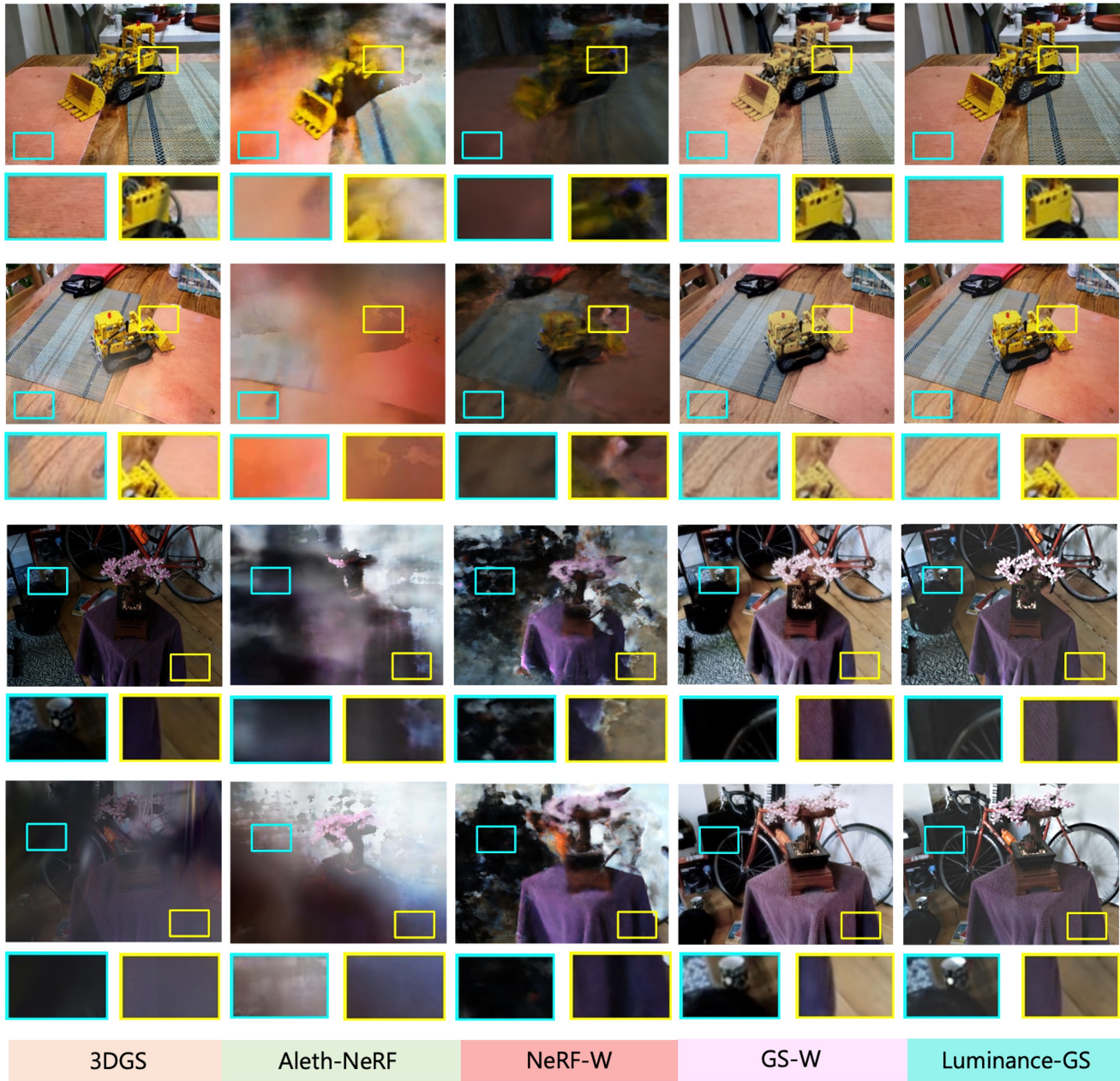


Figure 11. Novel view synthesis results on our synthesized varying exposure unbounded dataset (from Mip-NeRF 360 dataset [2]) “kitchen” and “bonsai” scenes, with comparison of 3DGS [29], Aleth-NeRF [15], NeRF-W [40] and GS-W [60].